Ice shelf rift propagation: stability, three-dimensional effects, and the role of marginal weakening

Bradley Paul Lipovsky

Department of Earth and Planetary Sciences
Harvard University

Correspondence: brad_lipovsky@fas.harvard.edu

Abstract. Understanding the processes that govern ice shelf extent are of fundamental importance to improved estimates of future sea-level rise. In present-day Antarctica, ice shelf extent is most commonly determined by the propagation of through-cutting fractures called ice shelf rifts. Here, I present the first three-dimensional analysis of ice shelf rift propagation. I present a linear elastic fracture mechanical (LEFM) description of rift propagation. The model predicts that rifts may be stabilized when buoyant flexure results in contact at the tops of the near-tip rift walls. This stabilizing tendency may be overcome, however, by processes that act in the ice shelf margins. In particular, both marginal weakening and the advection of rifts into an ice tongue are shown to be processes that may trigger rift propagation. Marginal shear stress is shown to be the determining factor that governs these types of rift instability. I furthermore show that rift stability is closely related to the transition from uniaxial to biaxial extension known as the compressive arch. Although the partial contact of rift walls is fundamentally a three-dimensional process, I demonstrate that it may be parameterized within more numerically efficient two-dimensional calculations. This study provides a step towards a description of calving physics that is based in fracture mechanics.

1 Introduction

The Antarctic ice sheet is projected to loose mass this century. Although the rates of mass loss over this timeframe are typically projected to mirror recent rates, several types of more extreme ice sheet response to global climate forcing cannot presently be excluded (Pattyn et al., 2018). Perhaps the most prominent of these extreme changes is the retreat of the floating ice shelves that fringe the Antarctic continent. Ice shelf retreat has been observed to occur gradually, i.e., over a period of years to decades (MacGregor et al., 2012; Arndt et al., 2018), and also abruptly, i.e., over a period of weeks to months (Scambos et al., 2000; Banwell et al., 2013). Although ice shelves themselves do not contribute to sea-level rise, they do act to buttress grounded ice (Rignot et al., 2004; Scambos et al., 2004; Goldberg et al., 2009; Gudmundsson, 2013). For this reason, ice sheet mass and therefore global mean sea-level are closely connected to the extent and stability of ice shelves. Here, I examine the stability of ice shelves with respect to the propagation of large through-cutting fractures called rifts.

The largest modern ice shelves exist in embayments. This basic observation has long prompted the notion that embayments promote the existence of large stable ice shelves (Hughes, 1977; Thomas and Bentley, 1978; Sanderson, 1979; Rist et al., 2002). Yet not all ice shelves fully fill the largest possible embayment. The Pine Island Glacier Ice Shelf, for example, does not presently fill the entire embayment between Bear Peninsula and Thurston Island; instead it fills the much smaller local embayment of Pine Island Bay. Furthermore, analysis of sediment cores (Naish et al., 2009; Marcott et al., 2011) and iceberg scour marks (Yokoyama et al., 2016) suggest that past ice shelves have waxed and waned in extent through ice age cycles. Although embayments appear to stabilize ice shelves, it would therefore appear that some other process is responsible for determining the size of a stable ice shelf within a given coastal geometry. The close relationship between the state of stress in an ice shelf and the ice shelf boundary conditions (Budd, 1966; Sanderson, 1979; MacAyeal, 1989) motivates investigation into processes acting in ice shelf margins.

Ice shelf margins are the part of the ice shelf grounding zone that is roughly parallel to flow (see Fig. 1). The importance of ice shelf margins is suggested by several observations, foremost among these being the observation of marginal weakening prior to ice shelf collapse. Estimates of ice rheology based on the inversion of surface velocity fields show extensive marginal weakening prior to the collapse of the Larsen A (Doake et al., 1998) and Larsen B Ice Shelves (Vieli et al., 2006; Khazendar et al., 2007). Although ice shelf collapse (i.e., total and rapid retreat) is a complex phenomenon that involves other processes besides rift propagation (Banwell et al., 2013), rift propagation does appear to play a role in collapse. Glasser and Scambos (2008) explicitly noted that marginal weakening immediately preceded rift propagation and eventual collapse on Larsen B. Further observation of a relationship between ice shelf retreat, rifting, and marginal thinning has been noted in the Amundsen Sea Embayment (MacGregor et al., 2012) and Jakobshavn Isbrae, Greenland (Joughin et al., 2008). Motivated by these observations, a central question of this paper is, what is the precise mechanical relationship between ice shelf margins and ice shelf rift propagation?

The main result of this paper is that marginal weakening can destabilize rift propagation. I begin by providing background on the state of stress in an ice shelf in Sections 2. In Section 3 I describe three-dimensional elasticity calculations that are carried out using the finite element method and then post-processed to reveal fracture mechanical properties. A more precise statement

of the main result is then given in Section 4, where I also examine a simplified analytical treatment of the three-dimensional calculations. I conclude by discussing the relationship between rift propagation, the compressive arch, rift-filling melange, and ocean swell in Section 5.

2 Background

I consider an ice shelf to be a buoyantly floating elastic plate of uniform thickness. Stress balance at the seaward-facing ice front results in both a net bending moment and an in-plane horizontal membrane stress (Weertman, 1957; Reeh, 1968). The vertically-averaged membrane stress is,

$$\sigma_m \equiv \frac{\rho g h}{2}\left(1 - \frac{\rho}{\rho_w}\right). \tag{1}$$

I use the $\equiv$ symbol to denote a definition. The bending moment is given by,

$$m_0 \equiv \frac{\rho g h^3}{12}\left[3\left(\frac{\rho}{\rho_w}\right) - 2\left(\frac{\rho}{\rho_w}\right)^2 - 1\right] \equiv \phi\frac{\rho g h^3}{12}. \tag{2}$$

In these expressions, ρ and ρ_w are the densities of ice and water and h is the ice thickness. Typical values of $\rho/\rho_w = 0.90$ give $\phi = 0.08$. The bending moment may also be expressed as a bending stress,

$$\sigma_b \equiv \frac{6 m_0}{h^2} = \phi\frac{\rho g h}{2}. \tag{3}$$

The bending stress σ_b is the value of the rift-normal stress at the top of the ice shelf; it is also the maximum value of the rift-normal stress. The horizontal component of loading (Eq. 1) is commonly used as a boundary condition in numerical ice flow models, whereas the bending moment is not typically applied in ice sheet models because its effects are confined to a narrow boundary layer in the vicinity of the ice front (MacAyeal, 1989).

Rifts walls have the same ice-front boundary conditions as a seaward-facing ice front. The main difference between a seaward-facing ice front and a rift wall is that it is possible for rift walls to come into contact. This contact is expected to occur at the top of the ice shelf and in the region near the rift tip, as illustrated in Fig. 1b. Indeed, De Rydt et al. (2018) recently observed that a rift tip on the Brunt Ice Shelf was further advanced at depth than at the surface, suggesting the occurrence of partial contact. I examine the partial contact of rift walls in Section 4. As an aspect of linear elastic fracture mechanics, fracture wall contact is a well-studied topic (Tada et al., 2000, Chapter 1, Section C).

I use three-dimensional elasticity calculations combined with linear elastic fracture mechanics (LEFM) to examine the propagation of ice shelf rifts. Although a number of previous studies have examined ice shelf rifts using LEFM, no previous study appears to have considered three-dimensional effects. Hulbe et al. (2010) calculated two-dimensional mixed mode (in-plane opening and shearing) stress intensity factors and as a result was able to state a fracture condition as well as predict rift propagation paths. Other ice shelf LEFM studies have mostly focused on propagation paths (Plate et al., 2012; Levermann et al., 2012; Borstad et al., 2017) and near-tip deformation (Larour et al., 2004a, b).

A final point of background concerns the relationship between the forces that drive fracture and the background ice flow. In real ice shelves, the state of stress is constantly evolving due to the change in geometry brought about by ice flow. Previous

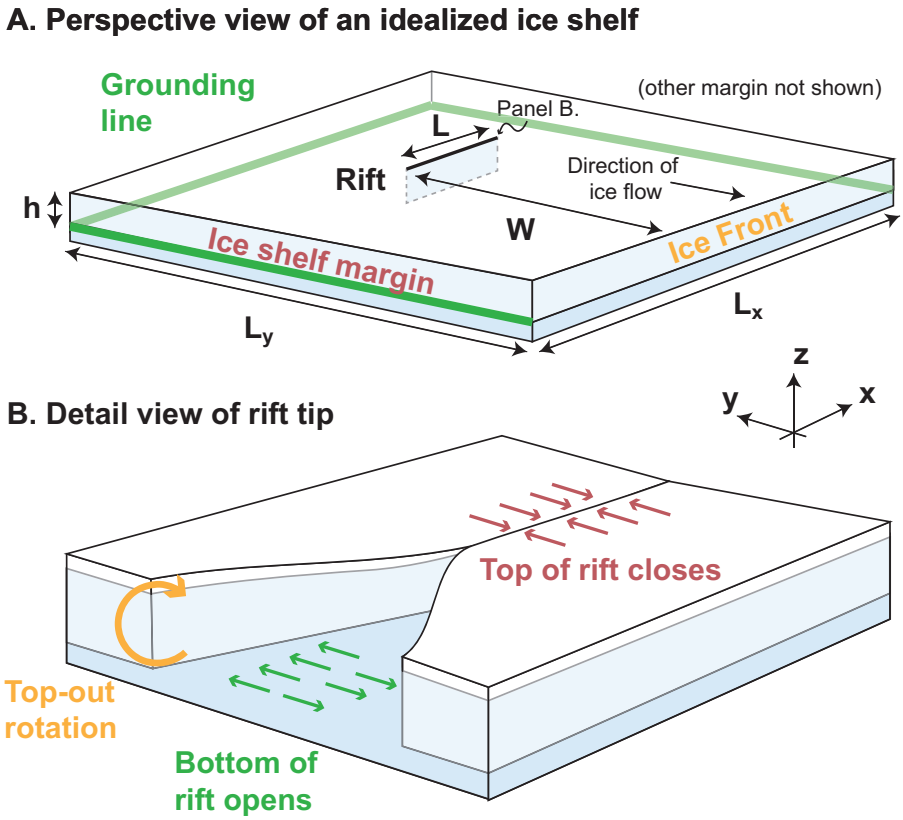

Figure 1. A. Simplified geometry of an idealized rectangular ice shelf. B. Zoomed in view of an ice shelf rift tip showing how buoyancy-driven rotation of the rift walls results in partial contact of the rift walls near the rift tip. Note that B. is drawn under the assumption that the rift tip is at least several flexural gravity wavelengths away from the ice shelf margin so that no flexural interaction occurs between these two regions.

studies have examined the relationship between ice flow and fracture in several ways. Hulbe et al. (2010) carried out viscous flow calculations to constrain the state of stress in their elastic calculations. They then tuned elastic moduli and boundary conditions in their elastic calculations to match the observed viscous stresses. Plate et al. (2012) parameterized a state of stress from a viscous flow model, but rather than tuning elastic moduli instead chose to introduce fictitious equivalent body forces. Here, I consider the hypothesis that the forces that drive rift propagation are entirely described by the instantaneous ice shelf geometry and boundary conditions. This hypothesis requires three-dimensional calculations in order to directly calculate – rather than parameterize or approximate– the role of gravitational driving forces. I therefore continue to describe the details of a three-dimensional elastic fracture model.

3 Mechanical Model

I begin this section by describing a three-dimensional elastic model of an ice shelf in which stresses and displacements are calculated using the finite element method (Sections 3.1 and 3.2). I then describe a linear elastic fracture model which is closely related to these elasticity calculations (Section 3.3).

3.1 Geometry

I consider the idealized ice shelf geometry shown in Fig. 1. The ice shelf is square in map view (the x-y plane). The z axis is defined so that the positive z axis points upwards and the bottom of the ice shelf is located at $z = 0$. The ice shelf has horizontal dimensions $L_x = L_y = 100$ km and thickness $h = 200$ m. The ice shelf surface at $y = 0$ faces the ocean and the surface at $y = L_y$ faces the ice sheet. The surfaces at $x = 0$ and $x = L_x$ are referred to as the ice shelf margins. A single rift is located along the x axis at $y = W$. I treat two different general rift locations: marginal and central. These two rift locations are shown in Fig. 2. I hold the rift length fixed at $L = 2.5$ km long for the marginal rift and $L = 5$ km long for the central rift.

Geometrically, I model a rift as a tapered rectangular hole in the ice shelf. Fractures in three dimensions have a fracture tip defined by a two-dimensional curve rather than a point. Although I refer to a rift tip for brevity, this term actually refers to a rift tip curve. In the treatment presented here, the rift tip curve is taken to be a vertical straight line. The rift is uniformly 10 m wide over most of its length. Simulations show negligible sensitivity to the choice of this width. Tapering is applied over a length equal to several widths (i.e., several tens of meters) near the rift tip.

3.2 Linear elasticity

I consider the equations of linear, homogeneous, isotropic, static, three-dimensional elasticity (Malvern, 1969),

$$\nabla \cdot \mathbf{T}' = -\rho \mathbf{g} \tag{4}$$

with total (Cauchy) stress tensor $\mathbf{T}'$, ice density ρ, and gravitational acceleration $\mathbf{g}$. Because I neglect any spatial variation in material parameters, my model does not include a firn layer.

I account for an initial hydrostatic stress in a manner following Cathles (2015) wherein the equations of elasticity are solved for a perturbation stress tensor $\mathbf{T}$ defined as the total (Cauchy) stress tensor minus the initial hydrostatic pressure,

$$\mathbf{T} \equiv \mathbf{T}' - p_0, \tag{5}$$

with,

$$p_0 \equiv \rho g (H - z) \tag{6}$$

The perturbation stress tensor is necessary for the following physical reason. Without subtracting the initial overburden pressure, the ice shelf experiences an initial volumetric contraction $\sim p_0/K$ with bulk modulus K. This volumetric contraction does not occur in real ice shelves because at time scales longer than the Maxwell time, ice is well approximated as being

incompressible (MacAyeal, 1989). Note that the perturbation stress tensor is not equal to the deviatoric stress tensor defined as $\mathbf{T}' - p$. This difference is important because the perturbation stress tensor accurately captures permissible, elastic volumetric contraction, whereas the deviatoric stress tensor does not.

All three-dimensional elasticity calculations in this study are carried out with respect to this perturbation stress tensor. The equations of motion are,

$$\nabla \cdot \mathbf{T} = 0 \tag{7}$$

$$T_{ij} = K\delta ij\epsilon_{kk} + 2\mu(\epsilon_{ij} + \delta_{ij}\epsilon_{kk}/3), \tag{8}$$

$$\epsilon_{ij} = \frac{1}{2}\left(\frac{\partial u_i}{\partial x_j} + \frac{\partial u_j}{\partial x_i}\right). \tag{9}$$

The first of these equations describes momentum balance which is derived by combining Eq. (5) and (6). Eq. (8) describes the elastic constitutive relation (Hooke's Law) with shear modulus $\mu = 3.6$ GPa and Poisson's ratio $\nu = 0.3$. Although isotropic elasticity only requires two elastic moduli, for convenience I use Young's modulus $E \equiv 2\mu(1+\nu)$ and the bulk modulus $K = E/[3(1-2\nu)]$. Eq. (9) defines the strain tensor ϵ_{ij}. These equation use index notation with repeated indices implying summation, δ_{ij} denoting the Kronecker delta function, and the indices i, j taking values x, y, z.

3.2.1 Boundary conditions

The ice front, rift walls, and top and bottom ice shelf surfaces are loaded by a depth-varying normal stress that is equal to the water pressure below the waterline and equal to zero above the waterline. These boundaries have zero applied shear stress. The water pressure condition may be written as,

$$\mathbf{n}^T \cdot (\mathbf{T}' \cdot \mathbf{n}) = -p_w(z), \tag{10}$$

with unit outward pointing normal vector $\mathbf{n}$, ice shelf draft $H_w \equiv \rho/\rho_w h$, and water pressure $p_w(z)$,

$$p_w(z) \equiv \begin{cases} \rho_w g\left[H_w - (z+w)\right] & z < H_w, \\ 0 & z \geq H_w. \end{cases} \tag{11}$$

Here, w is the vertical component of the displacement vector. This boundary condition is consistent with previous treatments of crevasse propagation in glaciers (e.g., Van der Veen, 1998).

In all simulations that are presented here, the surface of the ice shelf above the grounding line at $y = L_y$ has a zero displacement boundary condition. Similarly, the ice shelf surface at the ice front at $y = 0$ has a water pressure boundary condition (Eq. 11). In the margins, I examine three types of marginal boundary condition. These conditions are shown in Fig. 2; they are:

1. Ice shelf with ice tongue: margins have zero displacement between $y = L_y/2$ and $y = L_y$ and have water pressure between $y = 0$ and $y = L_y/2$;

2. Ice shelf in an embayment with strong margins: margins have zero displacement boundary condition; and,

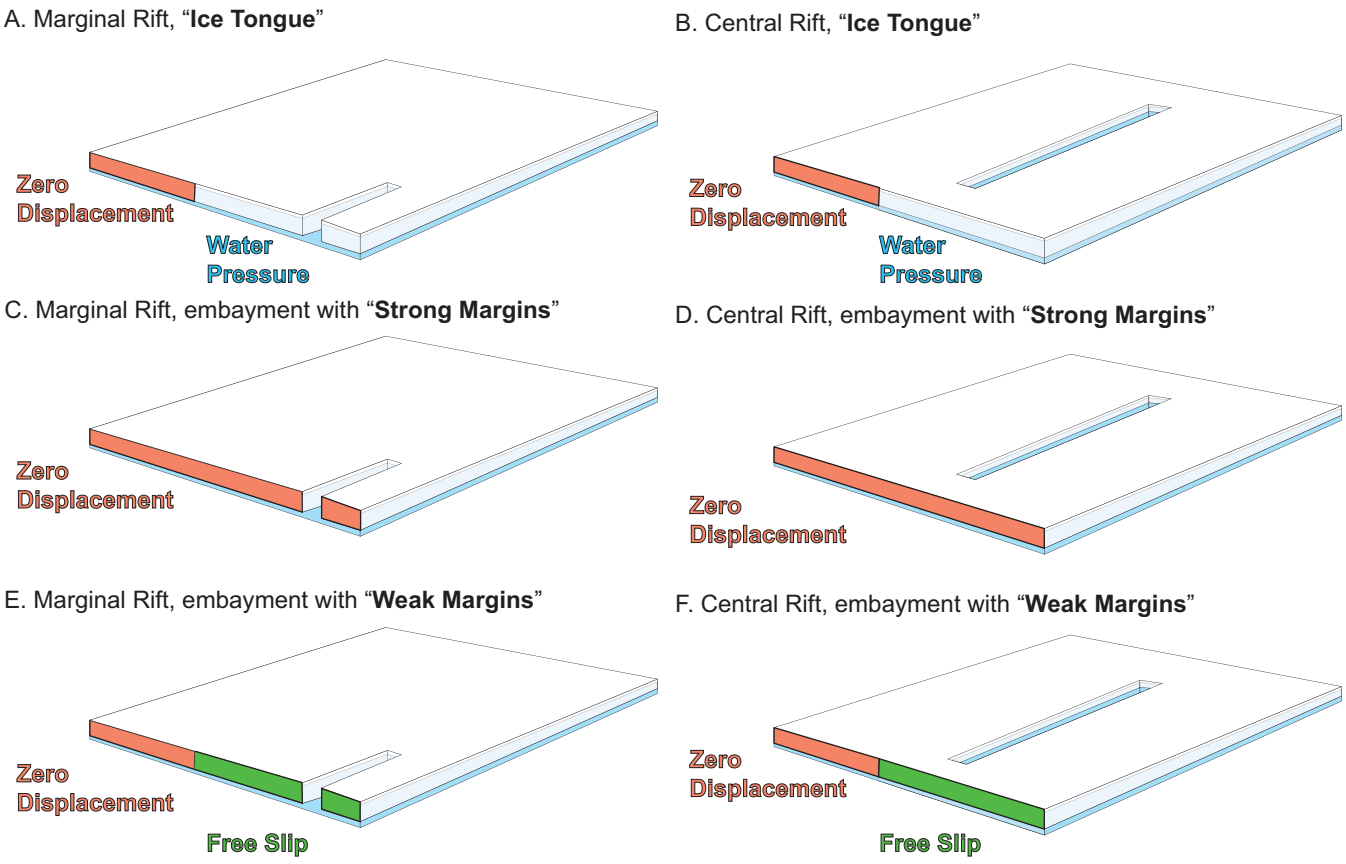

Figure 2. The geometries and boundary conditions considered in this study include: A. and B., Half zero displacement and half water pressure conditions; C. and D., entirely zero displacement conditions; and, E. and F., half zero displacement and half free slip conditions. I furthermore consider rifts that occur in the margins (A., C., and E.) and central rifts (B., D., and F.). The figures are not drawn to scale and the rift width is greatly exaggerated.

3. Ice shelf in an embayment with weak margins: margins have zero displacement between $y = L_y/2$ and $y = L_y$ and have zero shear stress and zero normal displacement between $y = 0$ and $y = L_y/2$.

Note that Equations 1-3 occur naturally as a result of the more general three-dimensional boundary conditions. Equations 1-3 are not applied as constraints in the three-dimensional calculations. They are used, however, in Section 4.1 to analytically approximate the numerical results.

3.2.2 Numerical implementation

I solve Eqs. 7-9 using the finite element method. The ice shelf domain is discretized using a free tetrahedral mesh in three spatial dimensions or a free triangular mesh in two spatial dimensions. In the three-dimensional simulations, the maximum element size along the rift is set to be $m \equiv h/16$. The element size then increases away from the rift to a maximum value

of 3.5 km. The rift is geometrically formed as a rectangular prism with width $W_{\text{rift}} = 10$ m and length L. I have verified that the results presented here have virtually no dependence on the choice of W_{rift} and m. In the two-dimensional simulations (described below), the maximum element size along the rift is $W_{\text{rift}}/10$.

3.3 Linear elastic fracture

Fractures in elastic materials create displacement fields that vary proportional to the distance r from the crack tip as $r^{1/2}$ (Irwin, 1957). The scalar constant of proportionality involves the stress intensity factor. Specifically, in terms of the displacement components u, v, and w corresponding to displacements in the x, y, and z directions, the stress intensity factors are defined through the relations (Tada et al., 2000),

$$u(r,z) = 4\frac{K_{II}(z)}{\mu/(1-\nu)}\sqrt{\frac{r}{2\pi}}, \tag{12}$$

$$v(r,z) = 4\frac{K_{I}(z)}{\mu/(1-\nu)}\sqrt{\frac{r}{2\pi}}, \tag{13}$$

$$w(r,z) = \frac{K_{III}(z)}{\mu}\sqrt{\frac{r}{2\pi}}. \tag{14}$$

The quantities K_I, K_{II}, and K_{III} are the Mode-I, Mode-II, and Mode-III stress intensity factors (SIFs). The sense of motion associated with each mode of fracture is shown in Fig. 3. Equations 12-14 represent the asymptotic value, accurate to first order, of the displacement field near the rift tip on the plane of the fracture. The stress intensity factors bear a direct relationship to fracture propagation.

A basic tenet of fracture mechanics is that unstable crack growth occurs when the elastic strain energy available to drive fracture exceeds the energy required to create new fracture area (Griffith, 1921). The key insight of linear elastic fracture mechanics is that this energy condition can be related to the stress intensity factors (Irwin, 1957). The stress intensity factors may therefore be used as part of a fracture criterion. In this study, I examine mixed-mode fracture and I therefore use the theory of Erdogan and Sih (1963) that calculates the single optimally-oriented stress intensity factor from the three different stress intensity modes. This optimally-oriented stress intensity factor is the Mode I stress intensity factor along a plane oriented to minimizes K_{II} and K_{III} (Erdogan and Sih, 1963; Hulbe et al., 2010). Under the assumption (verified later) that K_{III} does not substantially contribute to the direction of propagation of the rift tip line, the Mode I stress intensity factor along the optimal angle of propagation θ can be written as,

$$K_I^{Op} \equiv \cos\left(\frac{\theta}{2}\right)\left[K_I\cos^2\left(\frac{\theta}{2}\right) - \frac{3}{2}K_{II}\sin\theta\right]. \tag{15}$$

In this expression, the angle of propagation θ is given by,

$$\theta \equiv -2\tan^{-1}\left[\frac{-2K_I + 2\sqrt{K_I^2 + 8K_{II}^2}}{8K_I I}\right]. \tag{16}$$

In the adopted sign convention, negative angles indicate the direction pointing away from the ice front and straight-ahead propagation occurs when $\theta = 0$. Note that care must be taken in selecting the correct quadrant for the $\tan^{-1}$ function.

The fracture propagation criteria may then be stated as,

$$K_I^{Op} > K_{Ic}, \tag{17}$$

where the value $K_{Ic} = 100\ \text{kPa}\sqrt{\text{m}}$, is the Mode I fracture toughness of ice (Rist et al., 2002). I refer to rifts that satisfy Eq. (17) as being unstable because they are expected to undergo some amount of propagation. Note that this does not necessarily mean that the rift will propagate in a way that will lead to a calving event. Propagation may stop, for example, before calving occurs. Rifts that do not satisfy Eq. (17) will be referred to as stable; such rifts are expected to close. This closure may result in partial contact of the rift walls, as discussed next.

3.3.1 Partial contact of rift walls

The partial contact of rift walls is a nonlinear phenomenon because it involves solving for the shape of the contacting region and therefore changing the region over which different boundary conditions are applied (Johnson and Johnson, 1987). Here, I treat a linear formulation of this problem wherein the Mode-I stress intensity factor K_I can take on positive or negative values. This situation is discussed in detail by Tada et al. (2000). For fractures with zero initial width, a negative K_I implies unphysical material overlap. I avoid this situation in my numerical simulations by giving the rift an initial nonzero opening as described in Section 3.1. This is consistent with the idea that rifts in ice shelves are probably not held open entirely by elastic stresses because they have deformed through creeping flow. Other studies have shown that accounting for contact nonlinearity results in minimal differences from the linear problem for long fractures with $L \gg \lambda$ (Liu et al., 1999), where λ is the ice shelf flexural wavelength. Given that many rifts do reach lengths $L \gg \lambda$ (Walker et al., 2013, 2015), the linear approximation may well prove adequate for many cases of glaciological interest.

3.3.2 Stress intensity factor calculations

Stress intensity factors are calculated using rift wall displacements and Equations 12-14. This evaluation method, essentially a post-processing step, is sometimes called the displacement correlation method (Zehnder, 2012) and has previously been used in glacier studies by Jimenez and Duddu (2018). I evaluate Equations 12-14 at a distance r from the crack tip that is at least several times m in order to achieve grid-size independence. In three dimensions, stress intensity factors are calculated at various heights through the ice shelf thickness, with the resulting calculations plotted in Fig. 3.

4 Results and Analysis

Fig. 3 shows a typical result of the finite element calculations. This figure shows that the Mode-I and Mode-III stress intensity factors are nearly linear with depth (i.e., Fig. 3A, B, and E), while the Mode-II stress intensity factor is nearly uniform with depth (i.e., Fig. 3D). This structure in the solutions permits an approximate parameterization of three-dimensional effects. Such a parameterization allows for a much less computationally costly, two-dimensional problem to be solved.

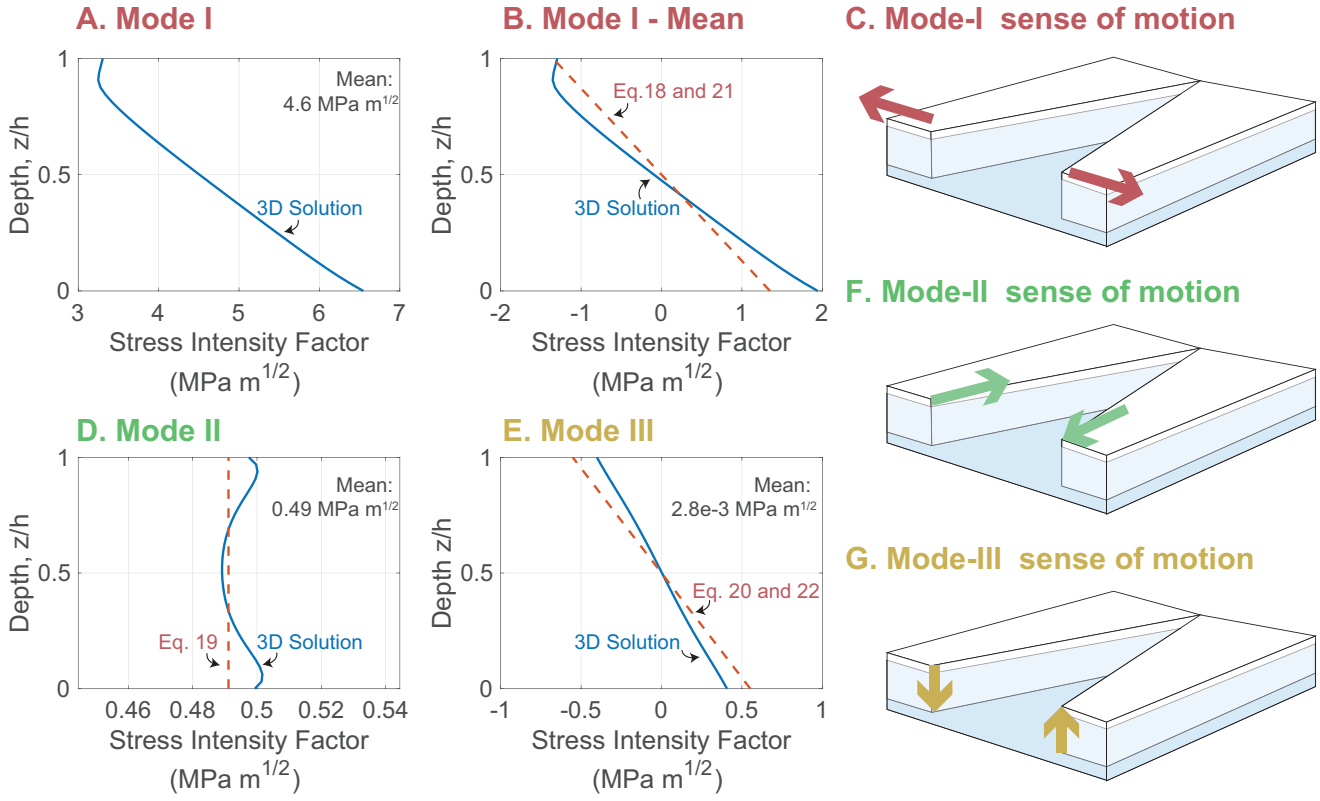

Figure 3. Typical three-dimensional stress intensity factors as a function of depth z in the ice shelf. A. and B. show the Mode I stress intensity factor K_I, D. shows the Mode II stress intensity factor K_{II} and E. shows the Mode III stress intensity factor K_{III}. The associated sense of motion for each mode is shown in panels C, F, and G. B. has the mean removed and is compared to the analytical solution of Eq. (21). The particular stress intensity factor solutions in these figures are plotted for a marginal rift in an ice tongue (i.e., the geometry shown in Fig. 2A.

I next develop the analytical parameterization (Section 4.1). After developing this 2D parameterization, I then apply it to examine the relationship between rift position and rift stability. Some readers may wish to skip directly to these results, which are given in Section 4.2.

4.1 Parameterization of 3D effects within 2D calculations

The structure of the three-dimensional stress intensity factors suggests the approximation,

$$K_I(z) = K_I^m + K_I^b \left(\frac{z - h/2}{h/2} \right), \tag{18}$$

$$K_{II}(z) = K_{II}^m, \tag{19}$$

$$K_{III}(z) = K_{III}^b \left(\frac{z - h/2}{h/2} \right), \tag{20}$$

Table 1. Comparison between 2D and 3D calculations

	h	2D	3D	m	(2D-3D)/3D
χ	100 m	-0.2937	-0.3127	12.5 m	-6.1%
	200 m	-0.2937	-0.3012	5 m	-2.5%
	200 m	-0.2937	-0.3069	12.5 m	-4.3%
ψ	100 m	-0.04408	-0.0385	12.5 m	+14.5%
	200 m	-0.04408	-0.0382	5 m	+15.4%
	200 m	-0.04408	-0.0379	12.5 m	+16.3%

where the superscripts b and m stand for bending and membrane, respectively. In the following, I calculate the bending components of the stress intensity factors K_I^b and K_{III}^b analytically and the membrane components K_I^m and K_{II}^m using two-dimensional finite element solutions.

4.1.1 The bending components of the SIFs

I find that the bending component of the Mode-I stress intensity factor is well fit by the previously-published stress intensity factor solution (Ang et al., 1963; Sih and Setzer, 1964; Folias, 1970; Sih, 2012),

$$K_I^b = -\sigma_b f(\nu)\sqrt{\lambda}. \tag{21}$$

Here, $\lambda^4 \equiv D/(\rho g)$ is the flexural length with flexural rigidity $D \equiv Eh^3/[12(1-\nu^2)]$. Hence, flexure results in a stabilizing contribution to the Mode I stress intensity factor that grows with ice thickness according to $K_I^b \sim h^{11/8}$. The bending stress σ_b is given by Eq. (3). The function $f(\nu)$ is discussed below. Notably, the bending stress intensity factors asymptotically vary with $\sqrt{\lambda}$ instead of the typical $\sqrt{L}$.

There is some discrepancy in the literature concerning the precise values of the function $f(\nu)$. Sih (2012) cites Folias (1970) who both note that f is of order unity but do not give its exact form. Ang et al. (1963) appears to have first given the dependence of f on ν although Sih and Setzer (1964) found a mistake in this work. Meanwhile, Bažant (1992) gives a different value of f. It appears, however, that Bažant (1992) did not correctly account for the rift-wall boundary condition. Given this uncertainty and the additional detail involved in the three-dimensional problem beyond the assumptions made by the above authors, I instead simply choose to calculate the value of $f(\nu)$ from the three-dimensional calculations. From these calculations, I find a value $f(\nu = 0.3) = 0.7646$. Of the above references, this value is most similar to the value calculated from the equation given by Sih and Setzer (1964), $f(\nu = 0.3) = 0.6063$.

Bending also creates a Mode-III stress intensity factor. Assuming that this bending can also be described within Euler beam theory, the Mode-III and Mode-I stress intensity factors are related by a factor,

$$\frac{K_{III}^b}{K_I^b} = \frac{h}{2\sqrt{2}(1+\nu)\lambda}. \tag{22}$$

Thus $K^b_{III} \sim h^2$, which is a larger exponent than for K^b_I. This solution was derived by assuming, consistent with Equations 12-14, that the ratio of stress intensity factors is proportional to the ratio of the stresses. This stress ratio is then calculated using the solution to the floating beam equation (Hetényi, 1971), $w = -2m_0/(\rho g \lambda^2)\exp(-x/\lambda)(\cos y/\lambda - \sin y/\lambda)$. The analytical solution of Eq. (22) is compared to the finite element solution in Fig. 3E (red dashed lines).

The analytical solution is not expected to perfectly match the finite element solution because the latter accounts for the full floatation condition (Eq. 10), whereas the bending model (Eq. 21) neglects higher order moments through Eq. (2). I further verify that the simplified model captures the behavior of the three-dimensional simulations by calculating stress intensity factors over a range of ice shelf thickness between 25 m and 1600 m. I find that $K^b_I \sim h^{1.31}$ in the three-dimensional calculations whereas $K^b_I \sim h^{1.375}$ analytically. Similarly, $K^b_{III}/K^b_I \sim h^{0.27}$ in the three-dimensional calculations whereas $K^b_{III}/K^b_I \sim h^{0.375}$ analytically. As can be seen in Fig. 3, the differences are more pronounced for K^b_{III}. I attribute the differences between analysis and calculation to the neglect of higher order moments and stress terms (i.e., the use of Euler beam theory).

4.1.2 The membrane components of the SIFs

I carry out simplified two-dimensional finite element calculations in order to describe the membrane components of the stress intensity factors. In two horizontal spatial dimensions x and y, the governing equations for the two-dimensional calculations are found by taking $\partial/\partial z = 0$ in Eqs. 7-9. In two spatial dimensions, the boundary condition on floating ice fronts takes the stress value given by Eq. (1).

I find good agreement between two-dimensional calculations and the depth-averaged values from three-dimensional calculations. Table 1 presents these results using the geometrical factors $\chi = K^m_I/(\sigma_m\sqrt{\pi L})$ and $\psi = K^m_{II}/(\sigma_m\sqrt{\pi L})$, where σ_m is the depth-integrated boundary condition given in Eq. (1). Note that $K_I \sim K_{II} \sim \sqrt{L}$ suggests that χ and ψ do not depend on L (Tada et al., 2000). The agreement is better for χ than for ψ, with differences on the order of several percent. This table also shows the effect of varying the maximum near-tip element length m. The values in this table are calculated for a central rift in an embayment with strong margins (i.e., as shown in Fig. 2D).

4.2 Central and Marginal Rifts

I now use the two-dimensional approach described in Section 4.1 to examine the effect of rift position on rift stability. I again consider all of the combinations of boundary conditions and rift locations shown in Fig. 2 while additionally varying the streamwise position of the rift W.

Stress intensity factors for marginal rifts are plotted in Fig. 4. These stress intensity factors were calculated using the 2D parameterization described in Section 4.1. Consistent with the shearing stresses experienced in the ice shelf margins, the Mode I and Mode II stress intensity factors are of similar magnitude (Fig. 4A and B, respectively). Fig. 4C shows that marginal rifts always tend to propagate in the direction away from the ice front, i.e., in the positive y direction (coordinates shown in Fig. 1).

Marginal rifts are unstable over the greatest range of locations in the ice tongue and weak margin geometries (Fig. 4D). Specifically, they become unstable at a position $W/L_y \approx 0.66$. Stability in these geometries is not spatially monotonic, however, and rifts again become stable near the ice front at $W/L_y \approx 0.33$. Marginal rifts in ice shelves with strong margins, in

contrast, have monotonically varying optimally oriented Mode I SIFs: they are stable near the grounding line and they become unstable at a distance $W/L_y \approx 0.33$ from the ice front.

Stress intensity factors for central rifts are plotted in Fig. 5. In contrast to the marginal rifts, central rifts have $|K_{II}| \ll |K_I|$ (Fig. 5A and B). Unlike marginal rifts, propagation angles are smaller, indicating nearly straight-ahead propagation (Fig. 5C). Furthermore, central rifts in all positions are found to have negative optimally oriented stress intensity factors indicative of stability (Fig. 5D).

5 Discussion

I have presented a three-dimensional LEFM analysis of ice shelf rift propagation. While this model has many potential applications, I have focused on the relationship between rift position and rift stability. In that regard, the main result of this analysis is that rifts originating in the margins of ice shelves become unstable if the ice shelf margin looses shear strength. This transition between a strong margin and a weak margin can be seen, for example, by comparing the red and yellow curves in Fig. 4D. Although this result is justified by the calculations presented in this paper, it is worth emphasizing several implicit and subtle assumptions.

I have assumed that margins have either zero displacement or zero shear stress. In reality, margins likely experienced reduced but nonzero shear stress. I have also considered only two rift locations (marginal or central), only one ice shelf geometry (square), and only one rift geometry (a single rift, perpendicular to flow, and without curvature). I treat the entire ice column as having identical material properties and therefore do not describe the firn layer and its relation to partial contact of rift walls. Additional observed rift-wall processes such as brine infiltration, surface accumulation, and variable uplift could also be investigated (Scambos et al., 2009, 2013; Walker and Gardner, 2019). Each of these assumptions deserves further examination. Despite these limitations, ice shelves and ice shelf rifts oftentimes approximately conform to the assumptions described in this study. I do therefore expect that the results presented here provide a useful basis for understanding rift propagation.

5.1 The compressive arch

All boundary conditions considered here give rise to a compressive arch, defined as the region where an ice shelf transitions from uniaxial to biaxial extension (Doake et al., 1998). The compressive arch can be visualized by plotting the second principle horizontal strain field, the first principle strain alway being positive (Fig. 6). Doake et al. (1998) proposed that "once a retreating ice front breaks through the critical 'compressive arch' then retreat is irreversible." The results presented here broadly confirm the hypothesis of Doake et al. (1998), although as shown in Section 4, the relation to the compressive arch only holds in an approximate sense. Specifically, for the strong margin boundary condition the onset of instability occurs somewhat upstream from the maximum extent of the compressive arch (Fig. 6A.). For the weak margins and ice tongue boundary conditions the agreement is closer, however, there is also a region of stability that occurs closer to the ice front (Fig. 6B. and C.).

Perhaps more importantly, the results presented here suggest a slightly different order of causality than that proposed by Doake et al. (1998). Rather than being an independent boundary that rifts may or may not propagate through, rift propagation

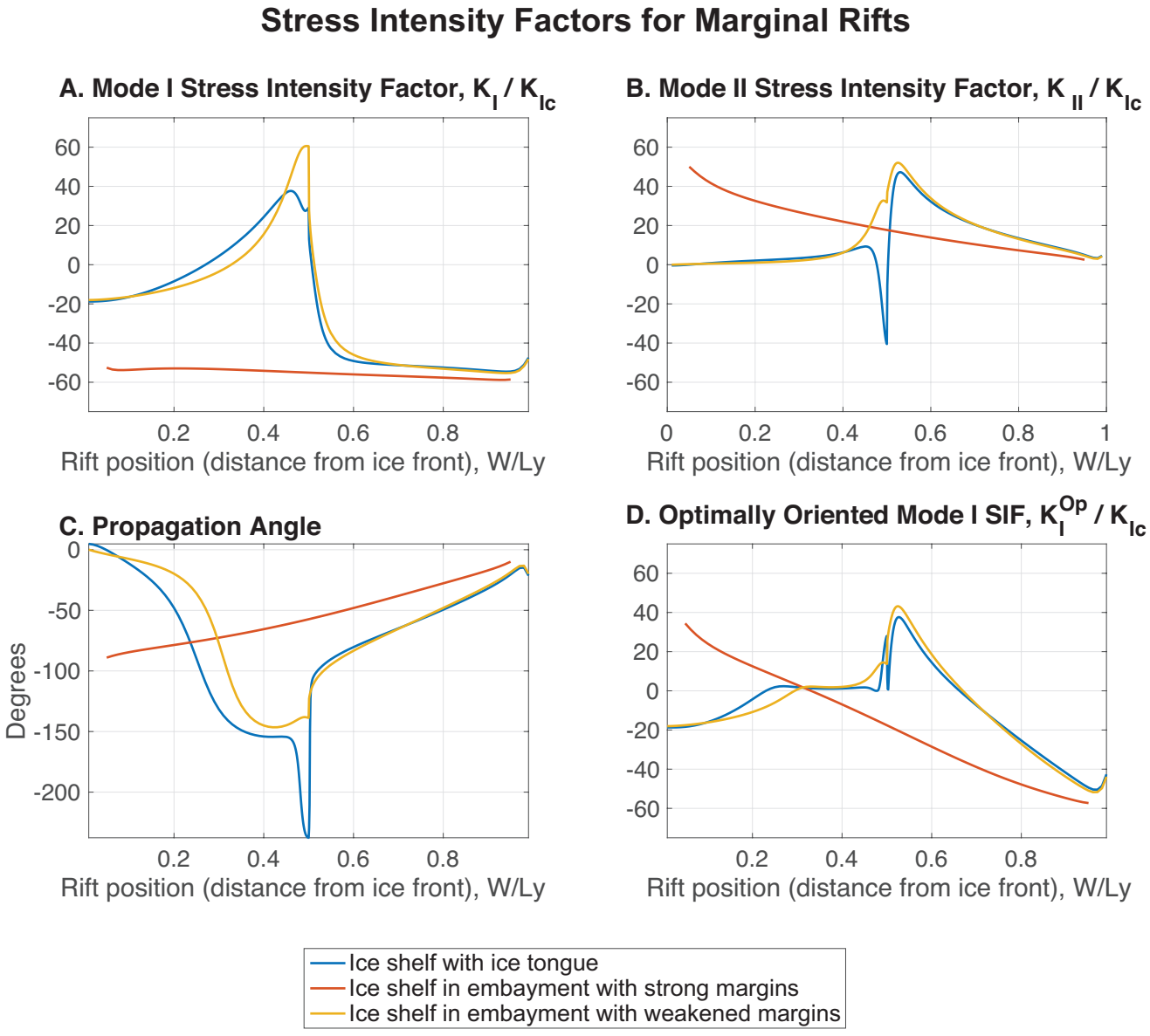

Figure 4. Stress intensity factors for marginal rifts may reflect either stability or instability depending on the position of the rift. Three pieces of information, the A. Mode I SIF, B. Mode II SIF, and C. Propagation angle, are combined using Eq. (15) to calculate D. the optimally-oriented SIF.

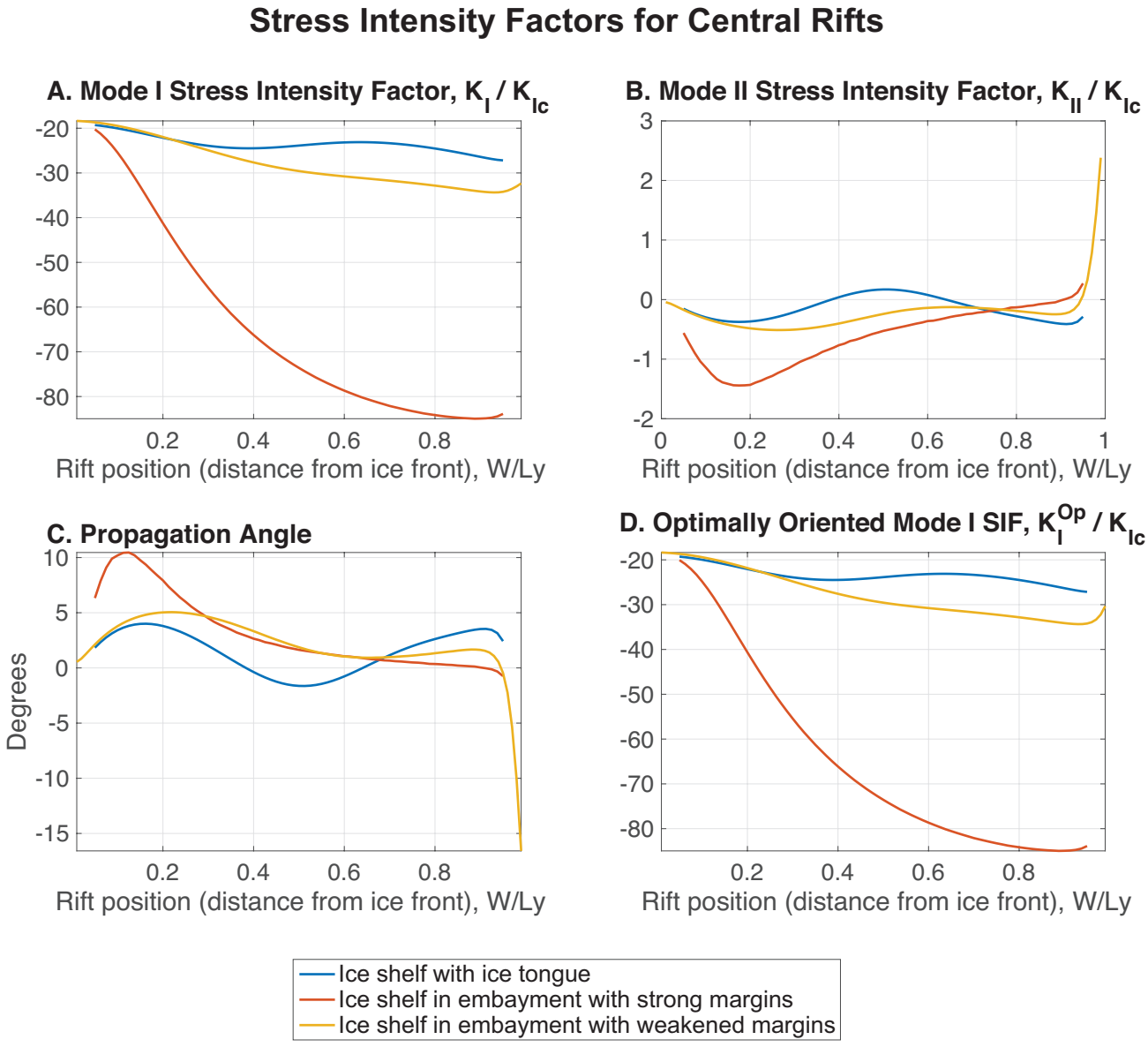

Figure 5. Stress intensity factors for central rifts reflect stability for all rift positions. Three pieces of information, the A. Mode I SIF, B. Mode II SIF, and C. Propagation angle, are combined using Eq. (15) to calculate D. the optimally-oriented SIF.

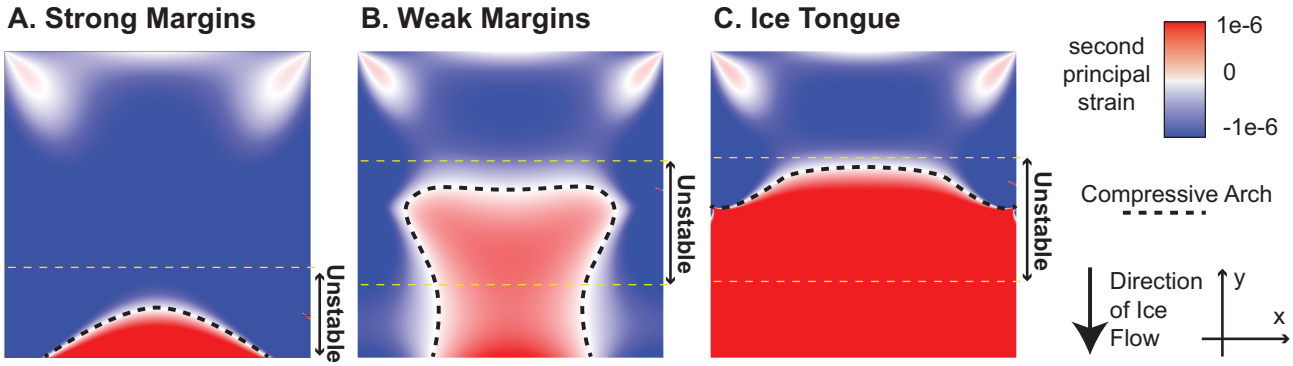

Figure 6. The ice shelf compressive arch (thick black dashed line) is plotted for three boundary conditions: A. Strong Margins, B. Weak Margins, and C. Ice Tongue (see Fig. 2). The figure also shows the boundaries of regions of rift instability (thin yellow dashed lines). These figures were calculated in two horizontal spatial dimensions as described in Section 4.1.2.

in the model presented here is expected to occur precisely because of the stress state that creates the compressive arch. Ice shelf retreat is expect to be irreversible only insofar as marginal weakening is itself irreversible.

5.2 Melange as a rift proppant

Olinger et al. (2019) observed a lack of rift-tip seismicity at central rift in the Ross Ice Shelf. This observation is consistent with the negative K_I^{Op} I have calculated for centrally-located rifts. In the absence of other forces such rifts will tend to close. It seems likely that these rifts therefore owe their continued existence to rift-filling melange that acts as a type of proppant by holding the rift open. Melange therefore has a dual nature. MacAyeal et al. (1998) and Rignot and MacAyeal (1998) showed that melange maintains shear stresses and therefore resists viscous flow. In this sense, melange is stabilizing. Yet in the sense that melange may sometimes enable the existence of rifts that would otherwise close, melange is destabilizing.

5.3 Wave-induced fracture

Lipovsky (2018) used passive seismic data to calculate the elastic ice shelf stresses due to ocean swell acting on the Ross ice shelf. This study concluded that some un-modeled process must have been operating in order to explain the lack of any observed ice shelf rift propagation during the observation period. Specifically, Lipovsky (2018) calculated a maximum wave-induced Mode-I stress intensity factor $K_I \approx 2$ MPa m$^{1/2}$ for a site near the Nascent Iceberg Rift. Using the results presented here for a central rift, we calculate that for a near-front central rift with $W/L_y = 0.05$, the Mode-I stress intensity without wave stress would be $K_I^{Op} \approx -5$ MPa m$^{1/2}$. The resulting total Mode-I stress intensity factor of $K_I^{Op} \approx -3$ MPa m$^{1/2}$ being negative is consistent with the observation that ocean swell did not trigger rift propagation during the observation period described by Lipovsky (2018).

6 Conclusion

I have modeled an ice shelf as a three-dimensional buoyantly floating elastic plate. I then show how these three-dimensional results may be captured in simplified two-dimensional calculations. Using the two-dimensional theory, I show that ice shelf rifts become unstable in the presence of marginal weakening or upon exiting an embayment. These results are a step towards prognostic ice shelf modeling with a physics-based relationship between ice dynamics and an ice front extent set by rift propagation.

Code and data availability. The analysis code used in the text is available on the author's GitHub repository.

Competing interests. The author declares that no competing interests are present.

Acknowledgements. This project began with a discussion with Colin Meyer at the Cambridge symposium of the International Glaciological Society in 2015. Jim Rice and Eric Dunham read earlier versus of this manuscript and gave the author helpful comments. Several discussions with Brent Minchew, Jan De Rydt, and Hilmar Gudmundsson also helped along the way. On a visit to C.U. Boulder organized by Jed Brown, David Marshall was critical of some early results; this feedback was helpful. The author was funded by the Department of Earth and Planetary Sciences at Harvard University.

References

Ang, D., Folias, E., and Williams, M.: The bending stress in a cracked plate on an elastic foundation', Journal of Applied Mechanics, 1963.

Arndt, J. E., Larter, R. D., Friedl, P., Gohl, K., Höppner, K., et al.: Bathymetric controls on calving processes at Pine Island Glacier, The Cryosphere, 12, 2039–2050, 2018.

Banwell, A. F., MacAyeal, D. R., and Sergienko, O. V.: Breakup of the Larsen B Ice Shelf triggered by chain reaction drainage of supraglacial lakes, Geophysical Research Letters, 40, 5872–5876, 2013.

Bažant, Z. P.: Large-scale thermal bending fracture of sea ice plates, Journal of Geophysical Research: Oceans, 97, 17 739–17 751, 1992.

Borstad, C., McGrath, D., and Pope, A.: Fracture propagation and stability of ice shelves governed by ice shelf heterogeneity, Geophysical Research Letters, 44, 4186–4194, 2017.

Budd, W.: The dynamics of the Amery ice shelf, Journal of Glaciology, 6, 335–358, 1966.

Cathles, L. M.: Viscosity of the Earth's Mantle, vol. 1362, Princeton University Press, 2015.

De Rydt, J., Gudmundsson, H., Nagler, T., Wuite, J., and King, E. C.: Recent rift formation and impact on the structural integrity of the Brunt Ice Shelf, East Antarctica, The Cryosphere, 12, 505–520, 2018.

Doake, C., Corr, H., Rott, H., Skvarca, P., and Young, N.: Breakup and conditions for stability of the northern Larsen Ice Shelf, Antarctica, Nature, 391, 778–780, 1998.

Erdogan, F. and Sih, G.: On the crack extension in plates under plane loading and transverse shear, Journal of basic engineering, 85, 519–525, 1963.

Folias, E.: On a plate supported by an elastic foundation and containing a finite crack, International Journal of Fracture Mechanics, 6, 257–263, 1970.

Glasser, N. and Scambos, T. A.: A structural glaciological analysis of the 2002 Larsen B ice-shelf collapse, Journal of Glaciology, 54, 3–16, 2008.

Goldberg, D., Holland, D., and Schoof, C.: Grounding line movement and ice shelf buttressing in marine ice sheets, Journal of Geophysical Research: Earth Surface, 114, 2009.

Griffith, A. A.: The phenomena of rupture and flow in solids, Philosophical Transactions of the Royal Society of London, 221, 163–198, 1921.

Gudmundsson, G.: Ice-shelf buttressing and the stability of marine ice sheets, The Cryosphere, 7, 647, 2013.

Hetényi, M.: Beams on elastic foundation: theory with applications in the fields of civil and mechanical engineering, BOOK, University of Michigan, 1971.

Hughes, T.: West Antarctic ice streams, Reviews of Geophysics, 15, 1–46, 1977.

Hulbe, C. L., LeDoux, C., and Cruikshank, K.: Propagation of long fractures in the Ronne Ice Shelf, Antarctica, investigated using a numerical model of fracture propagation, Journal of Glaciology, 56, 459–472, 2010.

Irwin, G. R.: Analysis of stresses and strains near the end of a crack traversing a plate, Journal of applied mechanics, 24, 361–364, 1957.

Jimenez, S. and Duddu, R.: On the evaluation of the stress intensity factor in calving models using linear elastic fracture mechanics, Journal of Glaciology, 64, 759–770, 2018.

Johnson, K. L. and Johnson, K. L.: Contact mechanics, Cambridge university press, 1987.

Joughin, I., Howat, I. M., Fahnestock, M., Smith, B., Krabill, W., Alley, R. B., Stern, H., and Truffer, M.: Continued evolution of Jakobshavn Isbrae following its rapid speedup, Journal of Geophysical Research: Earth Surface, 113, 2008.

Khazendar, A., Rignot, E., and Larour, E.: Larsen B Ice Shelf rheology preceding its disintegration inferred by a control method, Geophysical Research Letters, 34, 2007.

Larour, E., Rignot, E., and Aubry, D.: Modelling of rift propagation on Ronne Ice Shelf, Antarctica, and sensitivity to climate change, Geophysical research letters, 31, 2004a.

Larour, E., Rignot, E., and Aubry, D.: Processes involved in the propagation of rifts near Hemmen ice rise, Ronne ice shelf, Antarctica, Journal of Glaciology, 50, 329–341, 2004b.

Levermann, A., Albrecht, T., Winkelmann, R., Martin, M. A., Haseloff, M., and Joughin, I.: Kinematic first-order calving law implies potential for abrupt ice-shelf retreat, The Cryosphere, 6, 273–286, 2012.

Lipovsky, B. P.: Ice Shelf Rift Propagation and the Mechanics of Wave-Induced Fracture, Journal of Geophysical Research: Oceans, 2018.

Liu, R., Wang, C., and Bathgate, R.: Crack closure in spherical shells, International Journal of Fracture, 1999.

MacAyeal, D. R.: Large-scale ice flow over a viscous basal sediment: Theory and application to ice stream B, Antarctica, Journal of Geophysical Research: Solid Earth, 94, 4071–4087, 1989.

MacAyeal, D. R., Rignot, E., and Hulbe, C. L.: Ice-shelf dynamics near the front of the Filchner-Ronne Ice Shelf, Antarctica, revealed by SAR interferometry: model/interferogram comparison, Journal of Glaciology, 44, 419–428, 1998.

MacGregor, J. A., Catania, G. A., Markowski, M. S., and Andrews, A. G.: Widespread rifting and retreat of ice-shelf margins in the eastern Amundsen Sea Embayment between 1972 and 2011, Journal of Glaciology, 58, 458–466, 2012.

Malvern, L. E.: Introduction to the Mechanics of a Continuous Medium, Monograph, 1969.

Marcott, S. A., Clark, P. U., Padman, L., Klinkhammer, G. P., Springer, S. R., Liu, Z., Otto-Bliesner, B. L., Carlson, A. E., Ungerer, A., Padman, J., et al.: Ice-shelf collapse from subsurface warming as a trigger for Heinrich events, Proceedings of the National Academy of Sciences, 108, 13 415–13 419, 2011.

Naish, T., Powell, R., Levy, R., Wilson, G., Scherer, R., Talarico, F., Krissek, L., Niessen, F., Pompilio, M., Wilson, T., et al.: Obliquity-paced Pliocene West Antarctic ice sheet oscillations, Nature, 458, 322, 2009.

Olinger, S., Lipovsky, B., Wiens, D., Aster, R., Bromirski, P., Chen, Z., Gerstoft, P., Nyblade, A., and Stephen, R.: Tidal and Thermal Stresses Drive Seismicity along a Major Ross Ice Shelf Rift, Geophysical Research Letters, 2019.

Pattyn, F., Ritz, C., Hanna, E., Asay-Davis, X., DeConto, R., Durand, G., Favier, L., Fettweis, X., Goelzer, H., Golledge, N. R., et al.: The Greenland and Antarctic ice sheets under 1.5° C global warming, Nature Climate Change, p. 1, 2018.

Plate, C., Gross, D., Humbert, A., and Müller, R.: Analysis of Calving Events in Antarctic Ice Shelves Using Configurational Forces, PAMM, 12, 155–156, 2012.

Reeh, N.: On the calving of ice from floating glaciers and ice shelves, Journal of Glaciology, 7, 215–232, 1968.

Rignot, E. and MacAyeal, D. R.: Ice-shelf dynamics near the front of the Filchner Ronne Ice Shelf, Antarctica, revealed by SAR interferometry, Journal of Glaciology, 44, 405–418, 1998.

Rignot, E., Casassa, G., Gogineni, P., Krabill, W., Rivera, A., and Thomas, R.: Accelerated ice discharge from the Antarctic Peninsula following the collapse of Larsen B ice shelf, Geophysical Research Letters, 31, 2004.

Rist, M., Sammonds, P., Oerter, H., and Doake, C.: Fracture of Antarctic shelf ice, Journal of Geophysical Research: Solid Earth, 107, 2002.

Sanderson, T.: Equilibrium profile of ice shelves, Journal of Glaciology, 22, 435–460, 1979.

Scambos, T., Fricker, H. A., Liu, C.-C., Bohlander, J., Fastook, J., Sargent, A., Massom, R., and Wu, A.-M.: Ice shelf disintegration by plate bending and hydro-fracture: Satellite observations and model results of the 2008 Wilkins Ice Shelf break-ups, Earth and Planetary Science Letters, 280, 51–60, 2009.

Scambos, T., Ross, R., Haran, T., Bauer, R., Ainley, D., Seo, K.-W., De Keyser, M., Behar, A., and MacAyeal, D.: A camera and multisensor automated station design for polar physical and biological systems monitoring: AMIGOS, Journal of Glaciology, 59, 303–314, 2013.

Scambos, T. A., Hulbe, C., Fahnestock, M., and Bohlander, J.: The link between climate warming and break-up of ice shelves in the Antarctic Peninsula, Journal of Glaciology, 46, 516–530, 2000.

Scambos, T. A., Bohlander, J., Shuman, C. u., and Skvarca, P.: Glacier acceleration and thinning after ice shelf collapse in the Larsen B embayment, Antarctica, Geophysical Research Letters, 31, 2004.

Sih, G. and Setzer, D.: Discussion: The Bending Stress in a Cracked Plate on an Elastic Foundation (Ang, DD, Folias, ES, and Williams, ML, 1963, ASME J. Appl. Mech., 30, pp. 245–251), Journal of Applied Mechanics, 31, 365–366, 1964.

Sih, G. C.: Plates and shells with cracks: a collection of stress intensity factor solutions for cracks in plates and shells, vol. 3, Springer Science & Business Media, 2012.

Tada, H., Paris, P. C., and Irwin, G. R.: The stress analysis of cracks, Handbook, Del Research Corporation, 2000.

Thomas, R. H. and Bentley, C. R.: A model for Holocene retreat of the West Antarctic ice sheet, Quaternary Research, 10, 150–170, 1978.

Van der Veen, C.: Fracture mechanics approach to penetration of surface crevasses on glaciers, Cold Regions Science and Technology, 27, 31–47, 1998.

Vieli, A., Payne, A. J., Du, Z., and Shepherd, A.: Numerical modelling and data assimilation of the Larsen B ice shelf, Antarctic Peninsula, Philosophical Transactions of the Royal Society A: Mathematical, Physical and Engineering Sciences, 364, 1815–1839, 2006.

Walker, C. and Gardner, A.: Evolution of ice shelf rifts: Implications for formation mechanics and morphological controls, Earth and Planetary Science Letters, 526, 115 764, 2019.

Walker, C., Bassis, J., Fricker, H., and Czerwinski, R.: Structural and environmental controls on Antarctic ice shelf rift propagation inferred from satellite monitoring, Journal of Geophysical Research: Earth Surface, 118, 2354–2364, 2013.

Walker, C. C., Bassis, J. N., Fricker, H. A., and Czerwinski, R. J.: Observations of interannual and spatial variability in rift propagation in the Amery Ice Shelf, Antarctica, 2002–14, Journal of Glaciology, 61, 243–252, 2015.

Weertman, J.: Deformation of floating ice shelves, Journal of glaciology, 3, 38–42, 1957.

Yokoyama, Y., Anderson, J. B., Yamane, M., Simkins, L. M., Miyairi, Y., Yamazaki, T., Koizumi, M., Suga, H., Kusahara, K., Prothro, L., et al.: Widespread collapse of the Ross Ice Shelf during the late Holocene, Proceedings of the National Academy of Sciences, 113, 2354–2359, 2016.

Zehnder, A. T.: Fracture mechanics, Springer, 2012.